Modelling the Solar Dynamo with a Dynamic Non-linearity

Suzanne Menice
Supervisor: Dr. Paul Bushby

April 29, 2014

Abstract

Using the idea of an interface dynamo, the purpose of my project is to create a simplified model for the magnetic field within the Sun. The field is highly turbulent and very active making it a source of great interest. Observations of sunspots over many years has enabled us to draw a detailed picture of the Sun's magnetic activity cycle and using a 2-D Cartesian system I will show how this cycle can be obtained using a dynamo. I am interested in the large-scale problem with long time scales. My aim is to investigate modulation and try to recreate this in my model.

Contents

Chapter 1

Introduction

1.1 The Sun and its structure

The Sun is a large, spherical body of gas, it has a diameter of over 1 million km and the temperature at the surface is 5778K, (see, e.g., Stix, 2002). As the biggest planet in our solar system and vital for supporting life on Earth, the Sun is an area of great interest for scientists and our knowledge is ever increasing. One of the biggest areas of interest is the Sun's magnetic field and this is the main point of interest for my report.

It is very well understood how energy is created within the Sun, it is through a process of nuclear fission in the core. The fusion of hydrogen into helium creates thermal energy which radiates outward through the radiative zone into the convection zone. This outer region of the Sun is convectively unstable and is an area of highly turbulent flow. The distinct layers of the Sun are shown in Figure 1.2. Below the convection zone is the tachocline, shown in red. This is the area of greatest interest when trying to create a dynamo model.

1.2 Differential Rotation

Due to the gaseous nature of the Sun, the equator rotates more rapidly than the poles, the equator rotates once every 25 days whilst the poles take over a month. This is called differential rotation and it takes place not just on the surface but within the Sun too. One of the biggest developments in recent times was the introduction of helioseismology. This involves using the propagating waves throughout the Sun to learn more about its invisible internal structure giving us a better understanding of the processes in the Sun. Using

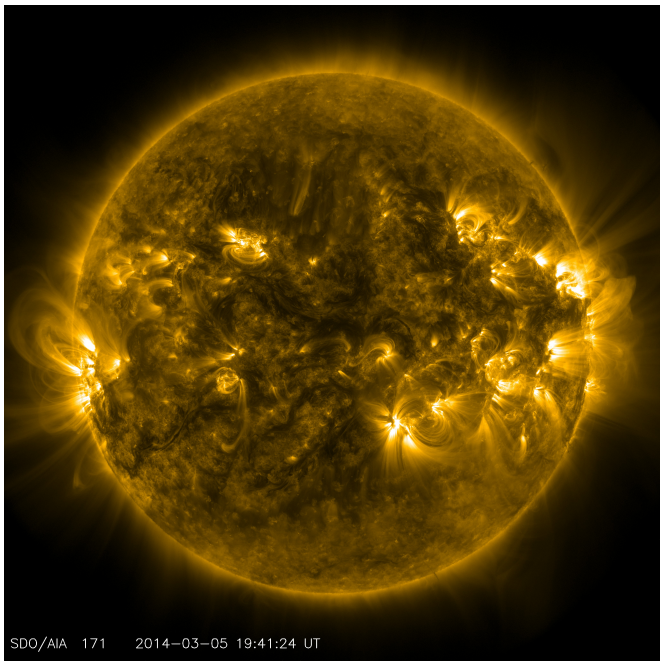

Figure 1.1: Image of the Sun, taken 5/3/14, Source - NASA Solar Dynamics Observatory

helioseismology it is possible to probe differential rotation within the solar interior. There is distinct variation in the angular velocity in different positions on the Sun; the angular velocity at high latitudes is know to be significantly smaller than the angular velocity at lower latitudes (Schou *et al.*, 1998). The changing velocities are depicted in Figure 1.3. This results in a strong radial shear which is mainly located in the tachocline.

Another important feature to consider are torsional oscillations, these are migrating bands of both faster than average and slower than average rotation. These are known as zonal flows. Helioseismology has been able to show that this occurs not just on the surface of the Sun but also underneath it, as deep as the outer 10% of the solar radius (Vorontsov *et al.*, 2002). The period of torsional oscillations is intrinsically linked with the period of the Sun's magnetic field and it's sunspots. The oscillations have a period of 11 years. In Figure 1.4 the red areas represent faster than average flows, whilst the blue areas show slower than average flows. It can be seen that during the cycle, the extreme values migrate to higher latitudes, i.e. towards the poles.

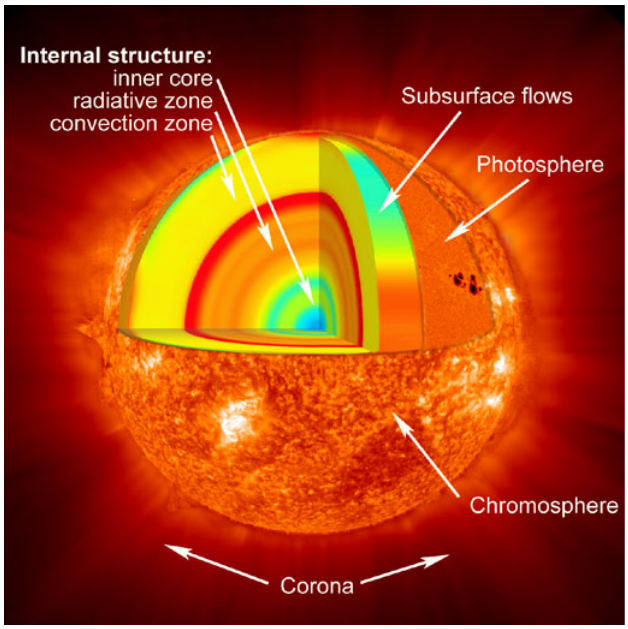

Figure 1.2: Internal Structure of the Sun, showing the convection zone, the radiative zone, and in between, the tachocline, shown in red. Source – NASA http://www.nasa.gov/mission˙pages/hinode/solar˙020.html

1.3 Magnetic observations

One of the most important and well documented observed features of the Sun is the occurrence of sunspots. Sunspots are very large pieces of magnetic flux that rise up to the solar surface due to a process called magnetic buoyancy. The size of each sunspot is equivalent to the size of the Earth. Observations have been recorded since the 17th century and they show that the number of sunspots varies over an eleven year cycle, see Figure 1.5. During each cycle the polarity reverses and so the complete magnetic cycle has a period of approximately 22 years. The data also shows that at the beginning of the cycle the sunspots appear predominantly at latitudes of around 30 °, known as the "zones of emergence" and then appear closer and closer to the equator as the cycle progresses (Tobias, 2002). The cycle is not completely periodic however, with clear variation and some very weak cycles and some strong cycles. The most obvious of these is known as the Maunder minimum, a period at the end of the 17th century where there was very little solar activity. When the solar activity started to increase again, the sunspots almost exclusively appeared in the southern hemisphere. At this time the Sun's field was strongly asymmetric whereas now it is dipolar - the azimuthal field is antisymmetric about the

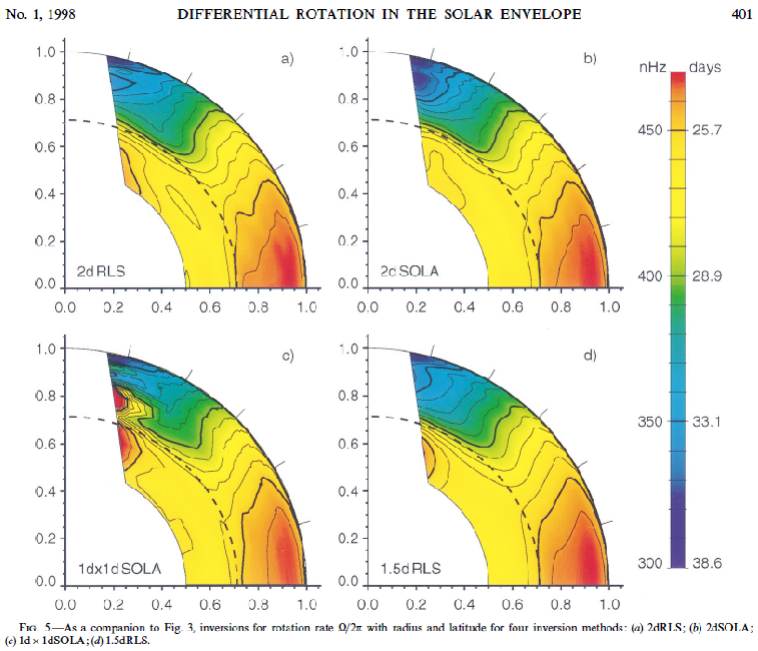

Figure 1.3: Differential Rotation in the Sun for contours of constant angular velocity. Taken from Schou *et al.* (1998)

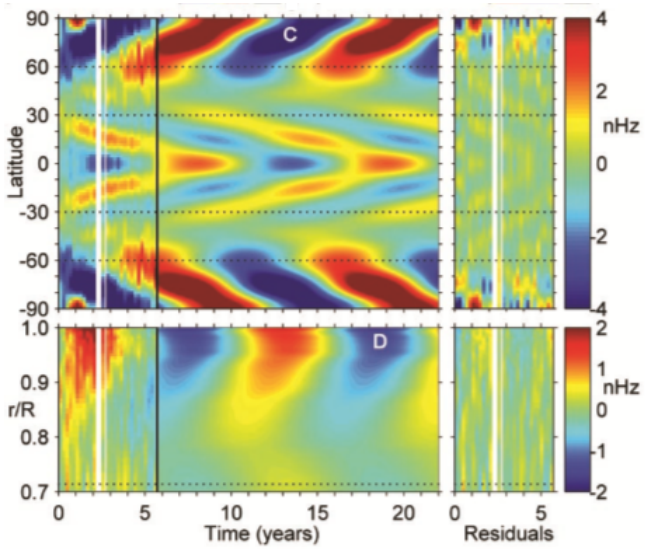

Figure 1.4: The top portion shows torsional oscillations: the rotational variation as a function of time and latitude at radius r. Red depicts faster than average flows and blue depicts slower than average flows. Taken from Vorontsov *et al.* (2002)

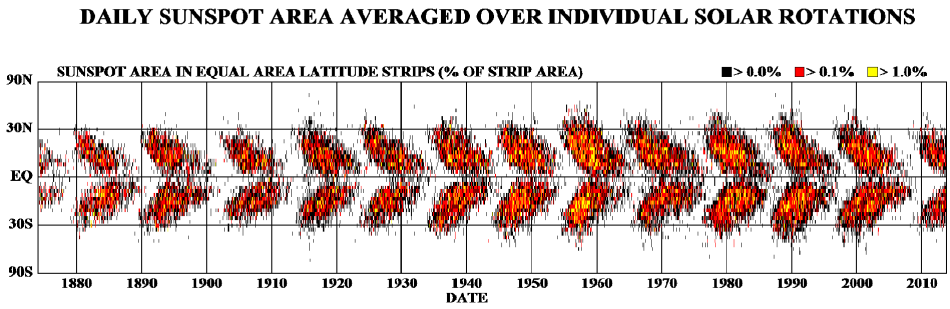

Figure 1.5: Butterfly diagram showing Sunspot activity, Source – NASA http://www.nasa.gov/vision/universe/solarsystem/solar˙cycle˙graphics˙prt.htm

equator whilst the poloidal potential is symmetric about the equator. The field may have been quadrupolar in the distant past but we can not be sure of this. A quadrupolar field is opposite to a diploar one, meaning that the azimuthal field is symmetric about the equator and the poloidal potential is a antisymmetric (see, e.g., Stix, 2002). In relatively recent times scientist have been able to accurately record the number of sunspots using observations of the Sun. By tracing the levels of ^{10}Be, found in ice cores, and ^{14}C, found in tree rings, whose abundance is anticorrelated to solar magnetic activity, scientist have also been able to deduce information about the history of the Sun's field and thus the number of sunspots from before direct observations began.

Chapter 2

Governing Equations

2.1 Basic Dynamo Theory

It is believed that the well observed cycle is caused by a large-scale dynamo. For this to be true, the Sun's magnetic field has to be continuously regenerated. The field can be regarded as being made up of poloidal and toroidal parts (see Figure 2.1). The poloidal part of the field runs from pole to pole, whilst the toroidal part runs around the equator. The process of converting the poloidal field into toroidal is called the ω-effect. This is caused by the differential rotation which 'stretches' out the poloidal field along around the sun. Conversely, the process of converting the toroidal field into the poloidal field is called the α-effect. This process is less well understood but it is thought that convection lifts loops of the field up and then the Coriolis force causes it to twist. These ideas form the basis of dynamo theory and I am going to assume that there is some form of dynamo located in the tacholine, between the Radiative and Convection zones, and this is given the name of an interface dynamo.

Scientists are investigating these types of models as they want to be able to predict what the Sun will do in the future. The magnetic field can affect satellites and other aspects of the earth's atmosphere. At present they are still unable to predict the cycle with any certainty. We are currently in cycle 24, it was thought it would be a strong cycle but has actually turned out to be quite weak (Dikpati *et al.*, 2006). Clearly this is an area where progress can still be made.

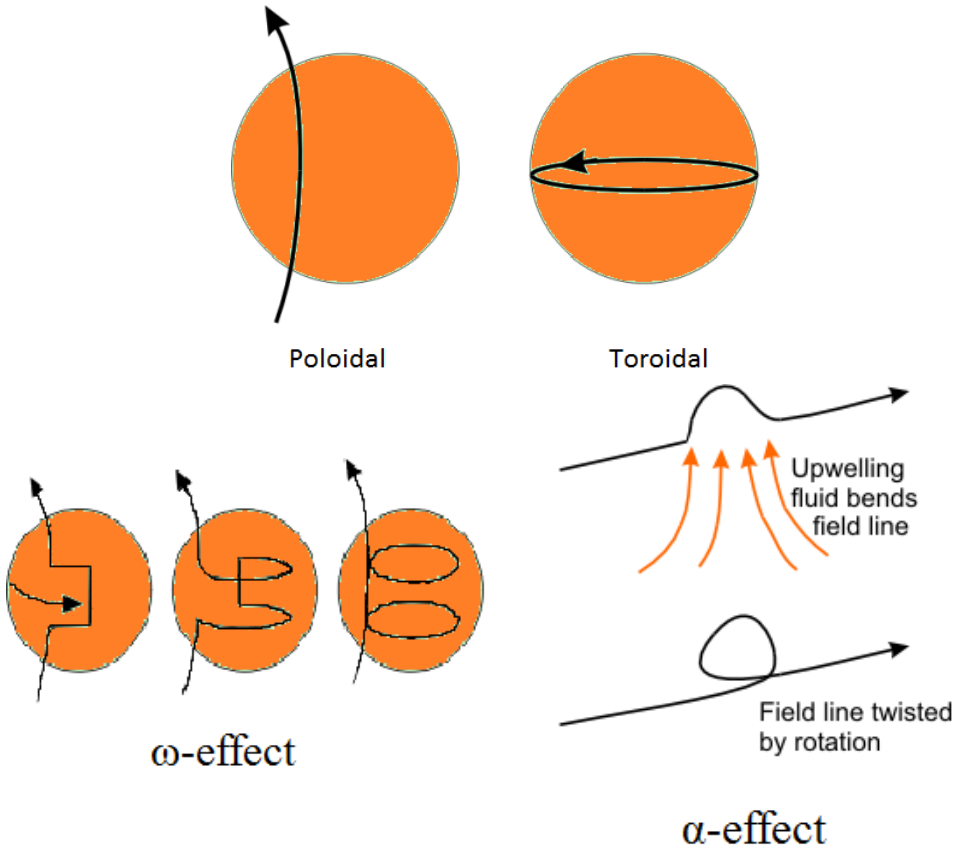

Figure 2.1: Top: the direction of the poloidal and toroidal fields. Bottom left: the conversion of poloidal into toroidal via stretching due to differential rotation. Bottom right: the conversion of toroidal into poloidal via the α-effect. Source – www.geomag.nrcan.gc.ca .

2.2 Maxwell's Equations

I begin with the well known Maxwell's equations which are:

$$\begin{aligned} \nabla \cdot \mathbf{B} &= 0, && (2.1)\\ \nabla \times \mathbf{B} &= \mu_0 \mathbf{j}, && (2.2)\\ -\frac{\partial \mathbf{B}}{\partial t} &= \nabla \times \mathbf{E}, && (2.3)\\ \mathbf{j} &= \sigma \left(\mathbf{E} + \mathbf{u} \times \mathbf{B} \right). && (2.4) \end{aligned}$$

Equation (2.2) is Ampère's Law, (2.3) is Faraday's Law and (2.4) is Ohm's Law. This form of Ohm's Law is slightly different to the standard form because the field is moving. Here, $\mathbf{B}(\mathbf{x}, t)$ represents the magnetic field, $\mathbf{E}(\mathbf{x}, t)$ is the electric field, $\mathbf{j}(\mathbf{x}, t)$ is the current density and $\mathbf{u}(\mathbf{x}, t)$ is the fluid velocity. Conventionally, μ_0 is the magnetic permeability and σ is the electric conductivity. I want to eliminate $\mathbf{E}$ and $\mathbf{j}$, this is done by substituting (2.4) into (2.2):

$$\begin{aligned} \nabla \times \mathbf{B} &= \mu_0 \sigma \left(\mathbf{E} + \mathbf{u} \times \mathbf{B} \right), && (2.5)\\ \nabla \times \left(\frac{1}{\mu_0 \sigma} \nabla \times \mathbf{B} \right) &= \nabla \times \mathbf{E} + \nabla \times \left(\mathbf{u} \times \mathbf{B} \right). && (2.6) \end{aligned}$$

Noticing that $\nabla \times \mathbf{E}$ is $-\partial \mathbf{B}/\partial t$ from (2.3) , I get the induction equation

$$\frac{\partial \mathbf{B}}{\partial t} = \nabla \times \left(\mathbf{u} \times \mathbf{B} \right) - \nabla \times \left(\frac{1}{\mu_0 \sigma} \nabla \times \mathbf{B} \right), \qquad (2.7)$$

$1/\mu_0 \sigma$ is defined as η, the magnetic diffusivity and I will assume it is constant. Thus the induction equation becomes

$$\frac{\partial \mathbf{B}}{\partial t} = \nabla \times \left(\mathbf{u} \times \mathbf{B} \right) - \eta \nabla \times \left(\nabla \times \mathbf{B} \right). \qquad (2.8)$$

Considering the last term, it can be simplified using suffix notation:

$$
\begin{aligned}
[\nabla \times (\nabla \times \mathbf{B})]_i &= \varepsilon_{ijk} \frac{\partial}{\partial x_j} (\nabla \times \mathbf{B})_k, && (2.9)\\
&= \varepsilon_{ijk} \frac{\partial}{\partial x_j} \left(\varepsilon_{kpq} \frac{\partial B_q}{\partial x_p} \right), && (2.10)\\
&= \varepsilon_{kij} \varepsilon_{kpq} \frac{\partial^2 B_q}{\partial x_j \partial x_p}, && (2.11)\\
&= (\delta_{ip}\delta_{jq} - \delta_{iq}\delta_{jp}) \frac{\partial^2 B_q}{\partial x_j \partial x_p}, && (2.12)\\
&= \frac{\partial^2 B_j}{\partial x_j \partial x_i} - \frac{\partial^2 B_i}{\partial x_j \partial x_j}, && (2.13)\\
&= \frac{\partial}{\partial x_i} \left(\frac{\partial B_j}{\partial x_j} \right) - \nabla^2 B_i, && (2.14)\\
&= \frac{\partial}{\partial x_i} (\nabla \cdot \mathbf{B}) - \nabla^2 B_i, && (2.15)\\
&= -\nabla^2 B_i. && (2.16)
\end{aligned}
$$

Thus (2.8) can be written as

$$\frac{\partial \mathbf{B}}{\partial t} = \nabla \times (\mathbf{u} \times \mathbf{B}) + \eta \nabla^2 \mathbf{B}. \tag{2.17}$$

I am interested in the large-scale field and so I will take averages using a Reynolds decompostion:

$$\mathbf{B} = \overline{\mathbf{B}} + \mathbf{b}' \qquad\qquad \mathbf{u} = \overline{\mathbf{u}} + \mathbf{u}', \tag{2.18}$$

where $\overline{\mathbf{B}}$ is the average and $\mathbf{b}'$ is the fluctuating part. This gives

$$
\begin{aligned}
\frac{\partial \overline{\mathbf{B}}}{\partial t} &= < \nabla \times (\mathbf{u} \times \mathbf{B}) > + \eta \nabla^2 \overline{\mathbf{B}}, && (2.19)\\
&= \nabla \times (\overline{\mathbf{u}} \times \overline{\mathbf{B}}) + \nabla \times < \mathbf{u}' \times \mathbf{b}' > + \eta \nabla^2 \overline{\mathbf{B}}. && (2.20)
\end{aligned}
$$

Assuming initially that $\mathbf{u}$ is given, then $\mathbf{b}'$ is linearly dependent upon $\overline{\mathbf{B}}$. Therefore, $< \mathbf{u}' \times \mathbf{b}' >$ is linearly dependent upon $\overline{\mathbf{B}}$. Further assuming that

$$< \mathbf{u}' \times \mathbf{b}' > = \alpha \overline{\mathbf{B}} - \beta \nabla \times \overline{\mathbf{B}}, \tag{2.21}$$

I can write,

$$\frac{\partial \overline{\mathbf{B}}}{\partial t} = \nabla \times (\overline{\mathbf{u}} \times \overline{\mathbf{B}}) + \nabla \times (\alpha \overline{\mathbf{B}}) + (\eta + \beta) \nabla^2 \overline{\mathbf{B}}. \tag{2.22}$$

This is the mean-field dynamo equation and it is fundamental to creating a dynamo model. Here α represents the α-effect as discussed in section 2.1 and β is enhanced turbulent diffusion.

Chapter 3

Cartesian System

3.1 System geometry

The basic form of my system is pictured in Figure 3.1. I have taken a thin layer around the tachocline running from pole to pole and flattened it out into a rectangular box. $x = 0$ represents the North Pole and $x = L$ represents the South Pole, therefore the equator lies at $x = L/2$. On the vertical axis, the domain runs from $z = 0$ to $z = l$ with the base of the convection zone situated at $z = l/2$.

3.2 Poloidal-Toroidal decomposition

Next, I need to derive equations for A and B whilst ensuring that $\nabla \cdot \mathbf{B} = 0$. Using (2.1), the poloidal-toroidal decomposition is

$$\mathbf{B} = B(x, z, t)\hat{\mathbf{y}} + \nabla \times [A(x, z, t)\hat{\mathbf{y}}]. \tag{3.1}$$

I assume that

$$\mathbf{u} = V(x, z)\hat{\mathbf{y}}, \quad \alpha \equiv \alpha(x, z), \quad \eta + \beta = \eta_T = constant. \tag{3.2}$$

The first term accounts for differential rotation whilst the last term is for simplicity. Thus,

$$\begin{aligned} \mathbf{B} &= B\hat{\mathbf{y}} + \nabla \times A\hat{\mathbf{y}}, & (3.3)\\ &= \left(-\frac{\partial A}{\partial z}, B, \frac{\partial A}{\partial x}\right). & (3.4) \end{aligned}$$

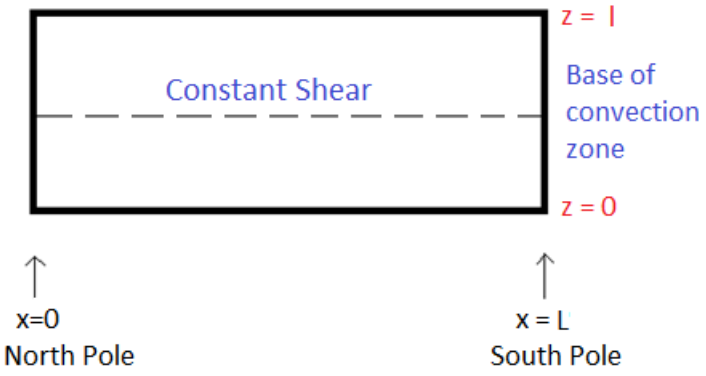

Figure 3.1: Simple diagram of system showing a flattened layer around the base of the convection zone from pole to pole.

Using this to calculate each part of (2.22)

$$\frac{\partial \mathbf{B}}{\partial t} = \left(-\frac{\partial}{\partial z}\left(\frac{\partial A}{\partial t}\right), \frac{\partial B}{\partial t}, \frac{\partial}{\partial x}\left(\frac{\partial A}{\partial t}\right)\right), \tag{3.5}$$

$$\mathbf{u} \times \mathbf{B} = \left(V\frac{\partial A}{\partial x}, 0, V\frac{\partial A}{\partial z}\right). \tag{3.6}$$

Thus,

$$\nabla \times (\mathbf{u} \times \mathbf{B}) = \left(0, \frac{\partial}{\partial z}\left[V\frac{\partial A}{\partial x}\right] - \frac{\partial}{\partial x}\left[V\frac{\partial A}{\partial z}\right], 0\right), \tag{3.7}$$

$$= \left(0, \frac{\partial V}{\partial z}\frac{\partial A}{\partial x} - \frac{\partial V}{\partial x}\frac{\partial A}{\partial z}, 0\right). \tag{3.8}$$

Similarly,

$$\nabla \times (\alpha \mathbf{B}) = \left(-\frac{\partial}{\partial z}(\alpha B), -\frac{\partial}{\partial z}\left[\alpha\frac{\partial A}{\partial z}\right] - \frac{\partial}{\partial x}\left[\alpha\frac{\partial A}{\partial x}\right], \frac{\partial}{\partial x}(\alpha B)\right), \tag{3.9}$$

and

$$\nabla^2 \mathbf{B} = \left(-\frac{\partial}{\partial z}(\nabla^2 A), \nabla^2 B, \frac{\partial}{\partial x}(\nabla^2 A)\right). \tag{3.10}$$

Combining the above 3 equations, I get

$$\frac{\partial A}{\partial t} = \alpha B + \eta_T \nabla^2 A, \tag{3.11}$$

$$\frac{\partial B}{\partial t} = \frac{\partial V}{\partial z}\frac{\partial A}{\partial x} - \frac{\partial V}{\partial x}\frac{\partial A}{\partial z} - \frac{\partial}{\partial z}\left(\alpha\frac{\partial A}{\partial z}\right) - \frac{\partial}{\partial x}\left(\alpha\frac{\partial A}{\partial x}\right) + \eta_T \nabla^2 B. \tag{3.12}$$

3.3 $\alpha-\omega$ Approximation and the Lorentz force

Before starting to analyse these equations numerically, it is best to simplify again. I am going to assume an $\alpha\omega$ approximation. This means that the ω effect is much stronger than the α effect, i.e. there is strong differential rotation. For my model this means neglecting α relative to the ∇V terms in (3.12). Therefore the mean field equations become

$$\frac{\partial A}{\partial t} = \alpha B + \eta_T \nabla^2 A, \tag{3.13}$$

$$\frac{\partial B}{\partial t} = \frac{\partial V}{\partial z}\frac{\partial A}{\partial x} - \frac{\partial V}{\partial x}\frac{\partial A}{\partial z} + \eta_T \nabla^2 B. \tag{3.14}$$

Motivated by observations of torsional oscillations I introduce a non-linearity, amending the system so that the flow is perturbed by the Lorentz force due to the magnetic field

$$\mathbf{F}_L \propto \frac{1}{\mu_0}(\nabla \times \mathbf{B}) \times \mathbf{B}. \tag{3.15}$$

Here I am assuming that all other forces are balanced an so any perturbation is due to the Lorentz force. The system becomes

$$\mathbf{u} = V(x,y)\hat{\mathbf{y}} + V'(x,z,t)\hat{\mathbf{y}}. \tag{3.16}$$

Using the Navier-Stokes equation I obtain a 3rd equation in my system governing V' (the perturbation to the azimuthal flow)

$$\rho\left(\frac{\partial \mathbf{u}}{\partial t} + (\mathbf{u}\cdot\nabla)\mathbf{u}\right) = -\nabla p + \rho\mathbf{g} + \mathbf{F} + \rho\nu\nabla^2\mathbf{u} + \mathbf{F}_m, \tag{3.17}$$

where $\mathbf{F}$ are imposed turbulent stresses and $\mathbf{F}_m$ is the Lorentz force. p is the pressure, ν is the kinematic viscosity, ρ is the density and $\mathbf{g}$ is the gravitational force. Taking the y-component of (3.17)

$$\frac{\partial V'}{\partial t} = \frac{1}{\rho}[\mathbf{j}\times\mathbf{B}]_y + \nu\nabla^2 V', \tag{3.18}$$

where

$$\mathbf{j} = \frac{1}{\mu_0}\nabla\times\mathbf{B}, \tag{3.19}$$

and

$$\mathbf{B} = \left(-\frac{\partial A}{\partial z}, B, \frac{\partial A}{\partial x}\right). \tag{3.20}$$

The RHS of (3.18) can be expanded component by component:

$$\nabla \times \mathbf{B} = \left(-\frac{\partial B}{\partial z}, -\frac{\partial^2 A}{\partial z^2} - \frac{\partial^2 A}{\partial x^2}, \frac{\partial B}{\partial x} \right). \tag{3.21}$$

Therefore

$$\mathbf{j} = \frac{1}{\mu_0} \left(-\frac{\partial B}{\partial z}, -\frac{\partial^2 A}{\partial z^2} - \frac{\partial^2 A}{\partial x^2}, \frac{\partial B}{\partial x} \right), \tag{3.22}$$

and

$$\begin{aligned} \mathbf{j} \times \mathbf{B} = \frac{1}{\mu_0} \Bigg(-\left(\frac{\partial^2 A}{\partial z^2} + \frac{\partial^2 A}{\partial x^2} \right) \frac{\partial A}{\partial x} - B\frac{\partial B}{\partial x}, -\frac{\partial B}{\partial x}\frac{\partial A}{\partial z} + \frac{\partial B}{\partial z}\frac{\partial A}{\partial x}, \\ -B\frac{\partial B}{\partial z} - \left(\frac{\partial^2 A}{\partial z^2} - \frac{\partial^2 A}{\partial x^2} \right) \frac{\partial A}{\partial z} \Bigg). \end{aligned} \tag{3.23}$$

Thus

$$[\mathbf{j} \times \mathbf{B}]_y = \frac{1}{\mu_0} \left(\frac{\partial B}{\partial z}\frac{\partial A}{\partial x} - \frac{\partial B}{\partial x}\frac{\partial A}{\partial z} \right), \tag{3.24}$$

and so (3.18) can be written as

$$\frac{\partial V'}{\partial t} = \frac{1}{\mu_0 \rho} \left(\frac{\partial B}{\partial z}\frac{\partial A}{\partial x} - \frac{\partial B}{\partial x}\frac{\partial A}{\partial z} \right) + \nu \nabla^2 V', \tag{3.25}$$

where again μ_0 is the magnetic permeability, ν is the kinematic viscosity and ρ is the density.

Now I have equations for $\partial A/\partial t$, $\partial B/\partial t$ and $\partial V'/\partial t$:

$$\frac{\partial A}{\partial t} = \alpha B + \eta_T \nabla^2 A, \tag{3.26}$$

$$\frac{\partial B}{\partial t} = \frac{\partial V}{\partial z}\frac{\partial A}{\partial x} - \frac{\partial V}{\partial x}\frac{\partial A}{\partial z} + \eta_T \nabla^2 B, \tag{3.27}$$

$$\frac{\partial V'}{\partial t} = \frac{1}{\mu_0 \rho} \left(\frac{\partial B}{\partial z}\frac{\partial A}{\partial x} - \frac{\partial B}{\partial x}\frac{\partial A}{\partial z} \right) + \nu \nabla^2 V'. \tag{3.28}$$

3.4 Dimensionless Equations

The next step is to make these dimensionless. To do this, I consulted Tobias (1996) and introduced the scalings:

$$\mathbf{x} = l\mathbf{x}^* \longrightarrow \nabla \sim \frac{1}{l}\nabla^* \longrightarrow \nabla^2 \sim \frac{1}{l^2}\nabla^{*2}, \tag{3.29}$$

$$t = \frac{l^2}{\eta_T} t^* \longrightarrow \frac{\partial}{\partial t} \sim \frac{\eta_T}{l^2} \frac{\partial}{\partial t^*}, \tag{3.30}$$

$$\alpha = \alpha_0 f(x,z), \quad A = l B_0 A^*, \quad B = B_0 B^*, \tag{3.31}$$

and

$$V = l\omega_0 V^*, \quad V' = l\omega_0 V'^*. \tag{3.32}$$

l is a characteristic lengthscale in the z-direction and α_0, ω_0 and B_0 are representative values. These correspond with my imposed boundary conditions of $A = B = V' = 0$ at $z = 0$ and $z = l$. Looking first at (3.26)

$$\frac{\eta_T}{l^2} l B_0 \frac{\partial A^*}{\partial t^*} = \alpha_0 B_0 f(x,z) B^* + \frac{\eta_T}{l^2} l B_0 \nabla^{*2} A^* \tag{3.33}$$

$$\frac{\partial A^*}{\partial t^*} = \frac{\alpha_0 l}{\eta_T} f(x,z) B^* + \nabla^{*2} A^* \tag{3.34}$$

Taking a further rescaling of

$$A^* = \frac{\alpha_0 l}{\eta_T} A^{**} \tag{3.35}$$

this becomes

$$\frac{\alpha_0 l}{\eta_T} \frac{\partial A^{**}}{\partial t^*} = \frac{\alpha_0 l}{\eta_T} f(x,z) B^* + \frac{\alpha_0 l}{\eta_T} \nabla^{*2} A^{**} \tag{3.36}$$

$$\frac{\partial A^{**}}{\partial t^*} = f(x,z) B^* + \nabla^{*2} A^{**} \tag{3.37}$$

A similar approach can be used to simplify (3.27) and (3.28), giving the following dimensionless equations,

$$\frac{\partial A}{\partial t} = f(x,z) B + \nabla^2 A \tag{3.38}$$

$$\frac{\partial B}{\partial t} = D \left[\frac{\partial (V + V')}{\partial z} \frac{\partial A}{\partial x} - \frac{\partial (V + V')}{\partial x} \frac{\partial A}{\partial z} \right] + \nabla^2 B \tag{3.39}$$

$$\frac{\partial V'}{\partial t} = sign(D) \left[\frac{\partial B}{\partial z} \frac{\partial A}{\partial x} - \frac{\partial B}{\partial x} \frac{\partial A}{\partial z} \right] + \tau \nabla^2 V' \tag{3.40}$$

Here, D is the dynamo number $\alpha_0 \omega_0 l^3 / \eta_T^2$ and $\tau = \nu / \eta_T$, the magnetic Prandtl number . $sign(D)$ takes the value -1 if $D < 0$ or $+1$ if $D > 0$.

Note that a further rescaling of A and B in (3.28) is needed to deal with the coefficient of the Lorentz force.

Chapter 4

Third Order System

4.1 Modifying the Equations

My aim is to use the model equations to reproduce the butterfly diagram showing the sunspot observations. I assume that $f(x,z) = F(x)$ and $A = B = V' = 0$ at $z = 0, l$ where $z = 0$ corresponds to the base of the domain and $z = l$ corresponds to the top. If I was using a spherical model, A, B and V' would all vanish at the poles to allow for the stress and current to be finite. In my 2-D model this corresponds to A, B and V' being zero at $x = 0$ and $x = L$. The assumption that they also vanish at $z = 0$ and $z = 1$ is simply an idealisation to make my model easier to solve. Using a similar approach to Dawes (2007), I introduce

$$A = A_1(x,t)\sin(\pi z), \tag{4.1}$$
$$B = B_1(x,t)\sin(\pi z), \tag{4.2}$$
$$V' = V_2(x,t)\sin(2\pi z), \tag{4.3}$$

and substituting these into (3.38), (3.39) and (3.40) then simplifying gives the equations for a third order coupled system. I have used $\sin(2\pi z)$ for the V' equation to allow for it being quadratic in B.

Looking in detail at the process for (3.40):

$$\begin{aligned}\frac{\partial}{\partial t}\left[V_2\sin(2\pi z)\right] = sign(D)\Bigg[&\frac{\partial}{\partial z}\left[B_1\sin(\pi z)\right]\frac{\partial}{\partial x}\left[A_1\sin(\pi z)\right] \\ &- \frac{\partial}{\partial z}\left[A_1\sin(\pi z)\right]\frac{\partial}{\partial x}\left[B_1\sin(\pi z)\right]\Bigg] \\ &+ \tau\frac{\partial^2}{\partial x^2}\left[V_2\sin(2\pi z)\right] + \tau\frac{\partial^2}{\partial z^2}\left[V_2\sin(2\pi z)\right]\end{aligned} \tag{4.4}$$

$$\sin(2\pi z)\frac{\partial V_2}{\partial t} = sign(D)\left[\pi\cos(\pi z)B_1\sin(\pi z)\frac{\partial A_1}{\partial x} - \pi\cos(\pi z)A_1\sin(\pi z)\frac{\partial B_1}{\partial x}\right] + \tau\sin(2\pi z)\frac{\partial^2 V_2}{\partial x^2} - 4\tau\pi^2\sin(2\pi z)V_2 \tag{4.5}$$

Using $\sin(2\pi z) = 2\sin(\pi z)\cos(\pi z)$,

$$\sin(2\pi z)\frac{\partial V_2}{\partial t} = sign(D)\left[\frac{\pi}{2}\sin(2\pi z)B_1\frac{\partial A_1}{\partial x} - \frac{\pi}{2}\sin(2\pi z)A_1\frac{\partial B_1}{\partial x}\right] + \tau\sin(2\pi z)\frac{\partial^2 V_2}{\partial x^2} - 4\tau\pi^2\sin(2\pi z)V_2 \tag{4.6}$$

Projecting onto the relevant Fourier mode gives

$$\frac{\partial V_2}{\partial t} = sign(D)\frac{\pi}{2}\left[B_1\frac{\partial A_1}{\partial x} - A_1\frac{\partial B_1}{\partial x}\right] + \tau\frac{\partial^2 V_2}{\partial x^2} - 4\pi^2\tau V_2 \tag{4.7}$$

This process can be similarly repeated for both (3.38) and (3.39). Therefore the equations for the 3rd order system are:

$$\frac{\partial A_1}{\partial t} = F(x)B_1 + \frac{\partial^2 A_1}{\partial x^2} - A_1\pi^2 \tag{4.8}$$

$$\frac{\partial B_1}{\partial t} = D\frac{\partial A_1}{\partial x} - \pi D\left[V_2\frac{\partial A_1}{\partial x} - \frac{A_1}{2}\frac{\partial V_2}{\partial x}\right] + \frac{\partial^2 B_1}{\partial x^2} - \pi^2 B_1 \tag{4.9}$$

$$\frac{\partial V_2}{\partial t} = sign(D)\frac{\pi}{2}\left[B_1\frac{\partial A_1}{\partial x} - A_1\frac{\partial B_1}{\partial x}\right] + \tau\frac{\partial^2 V_2}{\partial x^2} - 4\pi^2\tau V_2 \tag{4.10}$$

4.2 Numerical Methods

The system equations are very difficult to solve analytically and so I will solve them numerically. I am using a Runge-Kutta time step, defined as

$$k_1 = hf(x_n, y_n), \tag{4.11}$$

$$k_2 = hf(x_n + \frac{1}{2}h, y_n + \frac{1}{2}k_1), \tag{4.12}$$

$$y_{n+1} = y_n + k_2 + O(h^3), \tag{4.13}$$

which is 2nd order accurate in time, and the method of finite differences, which is 2nd order accurate in space along provided I use a time-step smaller than

$(\delta x)^2/2$, (Press *et al.*, 1986). This gives me my equations in a form suitable to solve in Fortran. For example, the RHS of (4.8) is written as

$$F(x)B_1(j) + \frac{A_1(j+1) - 2A_1(j) + A_1(j-1)}{(\Delta x)^2} - A_1(j)\pi^2 \tag{4.14}$$

I have also calculated the toroidal magnetic energy and kinetic energy of the system. The magnetic energy can be found using

$$\begin{aligned} E_M &= \frac{1}{2}\int_0^1 \int_0^8 \left[B_1(x,t)\sin(\pi z)\right]^2 \,\mathrm{d}x\mathrm{d}z, && (4.15)\\ &= \frac{1}{4}\int_0^1 \int_0^8 B_1^2\left[1-\cos(2\pi z)\right]\,\mathrm{d}x\mathrm{d}z, && (4.16)\\ &= \frac{1}{4}\int_0^8 B_1^2\left[z - \frac{1}{2\pi}\sin(2\pi z)\right]_0^1 \mathrm{d}x, && (4.17)\\ &= \frac{1}{4}\int_0^8 B_1^2\,\mathrm{d}x. && (4.18) \end{aligned}$$

Using the trapezium rule

$$\int_{x_0}^{x_n} f(x)\,\mathrm{d}x = \frac{1}{2}h\left[f(x_0) + f(x_n) + 2\left(f(x_1) + f(x_2) + \ldots + f(x_n - 1)\right)\right], \tag{4.19}$$

(4.18) becomes

$$E_M = \frac{\Delta x}{2}\left[\frac{1}{4}B_1(0)^2 + \frac{1}{4}B_1(N)^2 + \frac{2}{4}\sum_{i=1}^{N-1} B_1(i)^2\right]. \tag{4.20}$$

At the boundaries, B_1 is taken to be zero and so

$$E_M = \frac{\Delta x}{4}\sum_{i=1}^{N-1} B_1(i)^2. \tag{4.21}$$

Similarly, the kinetic energy is found from

$$E_K = \frac{1}{2}\int_0^1 \int_0^8 \left[V_2(x,t)\sin(\pi z)\right]^2 \,\mathrm{d}x\mathrm{d}z, \tag{4.22}$$

and so,

$$E_K = \frac{\Delta x}{4}\sum_{i=1}^{N-1} V_2(i)^2. \tag{4.23}$$

I am also interested in looking at the torsional oscillations and so calculate the average part of the induced flow. This requires taking the average of V_2 at each time step.

Another way to find the critical value of D is to consider the linear theory. The linearised equations for the system are

$$\frac{\partial A}{\partial t} = \cos\left(\frac{\pi x}{L}\right) B + \frac{\partial^2 A}{\partial x^2} - A\pi^2, \tag{4.24}$$

$$\frac{\partial B}{\partial t} = D\frac{\partial A}{\partial x} B + \frac{\partial^2 B}{\partial x^2} - B\pi^2, \tag{4.25}$$

$$\frac{\partial V}{\partial t} = \tau\frac{\partial^2 V}{\partial x^2} - 4\pi^2\tau V. \tag{4.26}$$

I am only interested in the A and B equations as they are coupled. Letting

$$A(x,t) = a_1(t)\sin\left(\frac{\pi x}{L}\right) + a_2(t)\sin\left(\frac{2\pi x}{L}\right), \tag{4.27}$$

and

$$B(x,t) = b_1(t)\sin\left(\frac{\pi x}{L}\right) + b_2(t)\sin\left(\frac{2\pi x}{L}\right), \tag{4.28}$$

and then substituting these into (4.24) and (4.25) then projecting onto each Fourier mode, first by multiplying the resultant equations by $\sin(\pi x/L)$ and integrating w.r.t x between 0 and L and then by multiplying the resultant equations by $\sin(\pi x/L)$ and integrating w.r.t x between 0 and L. Looking for solutions proportional to e^{pt} where $p \in \mathbb{C}$ by letting

$$a_1 = \hat{a}_1 e^{pt} \quad \text{and} \quad a_2 = \hat{a}_2 e^{pt}, \tag{4.29}$$

$$b_1 = \hat{b}_1 e^{pt} \quad \text{and} \quad b_2 = \hat{b}_2 e^{pt}, \tag{4.30}$$

where $p = \sigma + i\omega$. This results in 4 equations

$$\hat{a}_1\left(pL + \frac{4\pi^2}{L} + \pi^2 L\right) = \hat{b}_1\frac{L}{2}, \tag{4.31}$$

$$\hat{a}_2\left(pL + \frac{\pi^2}{L} + \pi^2 L\right) = \hat{b}_2\frac{L}{2}, \tag{4.32}$$

$$\hat{b}_1\left(pL + \frac{\pi^2}{L} + \pi^2 L\right) = \hat{a}_1\frac{16D}{3}, \tag{4.33}$$

$$\hat{b}_2\left(pL + \frac{4\pi^2}{L} + \pi^2 L\right) = -\hat{a}_1\frac{8D}{3}. \tag{4.34}$$

These equations can then be formed into a matrix and solved for D using Matlab.

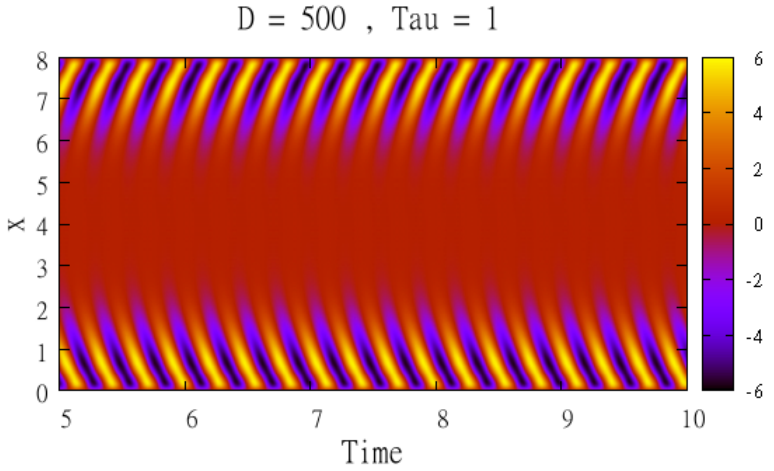

Figure 4.1: Contours of B_1 and x over time when $D = 500$ and $\tau = 1$

4.3 Numerical results

I was able to produce graphs that show x and B_1 varying over time. By plotting x, t and the mid-point of B1 I can reproduce the butterfly diagram, Figure 1.5. I also let $F(x) = \cos(\pi x/L)$.

I first looked at the case of $D > 0$ with $\tau = 1$. Figure 4.1 shows the contours of B1 over time when $D + 500$ and $\tau = 1$. They are clearly periodic and symmetric, however, the direction of propagation is polewards and this is the opposite to what we observe on the sun. Now looking at the case $D < 0$ as shown below, the propagation changes direction and so is in agreement with what actually happens in the sun. Thus I will look more closely at the negative D case.

I want to find the critical value for D by looking at the case $\tau = 1$. This is the simplest case because the time-scale is the same as the diffusive time-scale. From Figure 4.2 it is clear that the critical value for D lies between -400 and -450. This value is constant for all values of τ. Keeping τ constant I can demonstrate the effects of decreasing D.

Figure 4.3 shows the contours of B_1 along with the values of magnetic and kinetic energy when $D = -1000$ when $\tau = 1$. The contours are clearly periodic and symmetric with an amplitude of around 15. The magnetic and kinetic energies settle down to a steady oscillation after the initial perturbation. Next, decreasing D to -1500, Figure 4.4 the contours look rather similar, however the amplitude has increased to 20. The values of magnetic and kinetic energies have also increased but again follow a similar shape. A much more dramatic

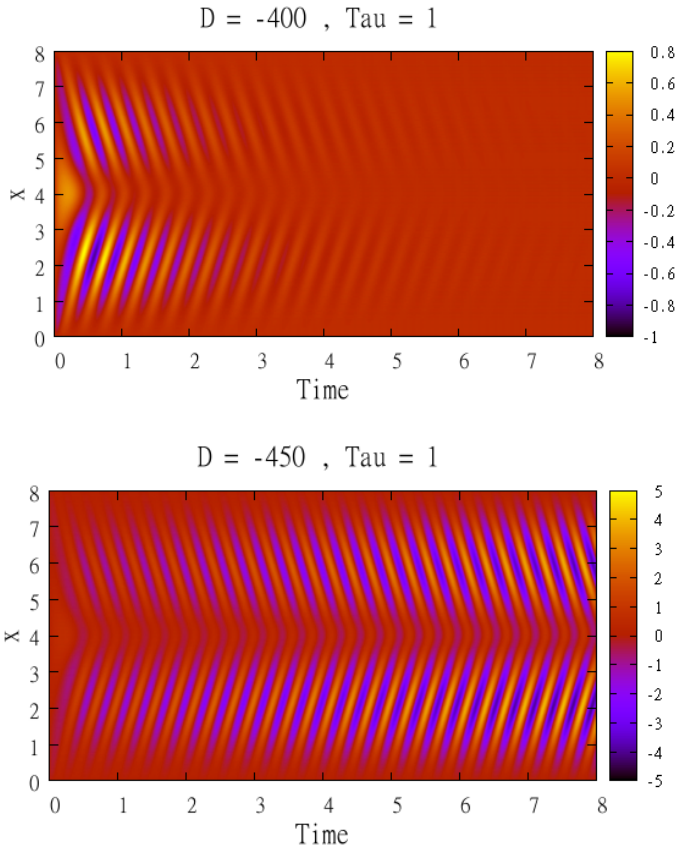

Figure 4.2: Contours of B_1 and x over time. Top; Decaying oscillations when $D = -400$, $\tau = 1$. Bottom: Growing oscillations when $D = -450$, $\tau = 1$.

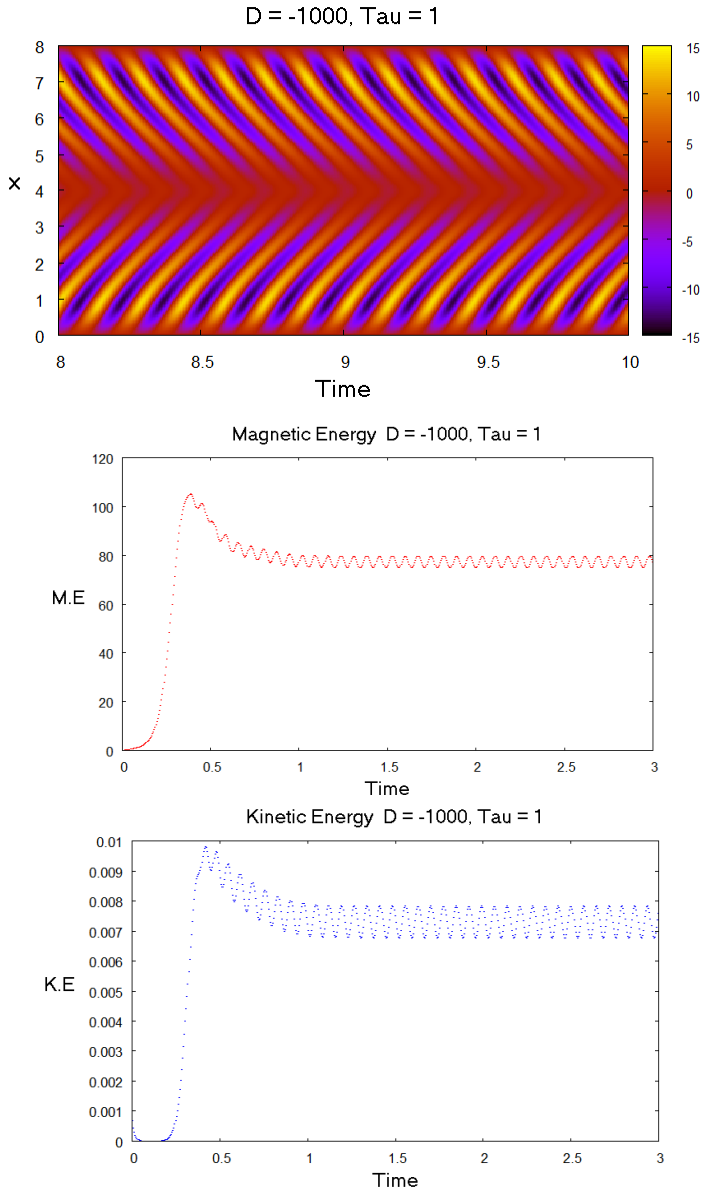

Figure 4.3: Top: Contours of B_1 and x over time when $D = -1000$ and $\tau = 1$. Middle: Magnetic energy. Bottom: Kinetic energy

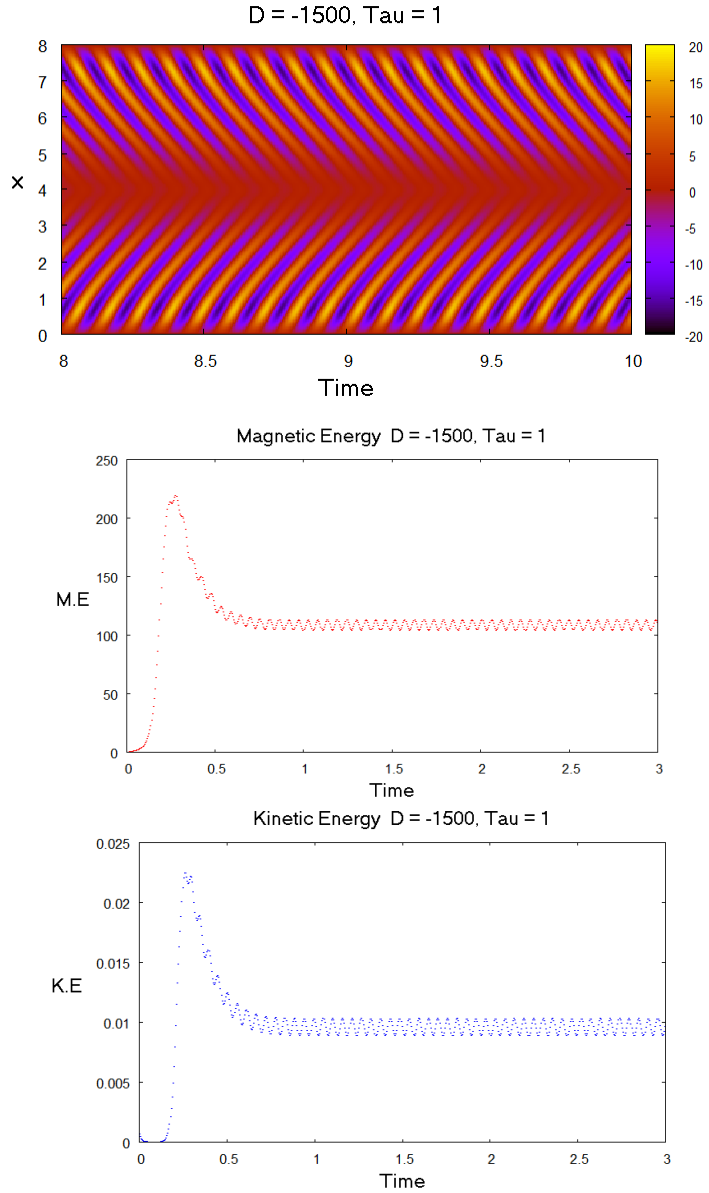

Figure 4.4: Top: Contours of B_1 and x over time when $D = -1500$ and $\tau = 1$. Middle: Magnetic energy. Bottom: Kinetic energy

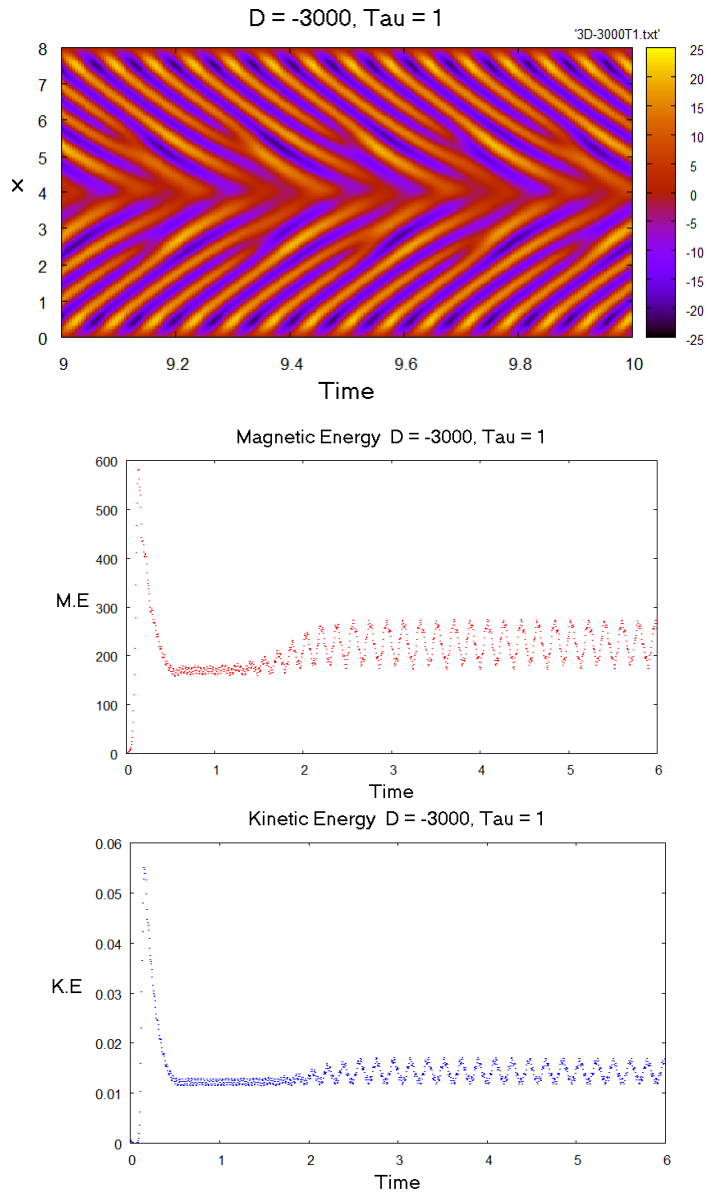

Figure 4.5: Top: Contours of B_1 and x over time when $D = -3000$ and $\tau = 1$. Middle: Magnetic energy. Bottom: Kinetic energy

change can be seen in Figure 4.5 when D decreases to -3000. The contours of B_1 are very asymmetric and the period has changed. Once again the amplitude has increased to 25 and the values of magnetic and kinetic have also increased, approximately by a factor of 2.

Below, I have shown the effects of decreasing τ whilst keeping D constant. Figure 4.6 shows the case when $D = 1000$ and $\tau = 0.1$. The contours are periodic and symmetric. It can been seen that after the initial perturbation, both the magnetic and kinetic energies settle down to a steady value. When I decreased τ to 0.025, as shown in Figure 4.7, the results are no longer symmetric. Looking at the energy graphs, the results are no longer steady, but appear to be roughly periodic. Decreasing τ once again, to 0.001, as in Figure 4.8, the contours are aperiodic and asymmetric. Both the magnetic and kinetic energy values no longer appear to follow any pattern and are unlike any of the previous graphs, they appear to be chaotically modulated.

The following graph shows the torsional oscillations for the third order system when $D = -1000$ and $\tau = 1$.

It is clear that the torsional oscillations follow the same shape as the contours of B_1. Looking at the graph we can count that there are approximately 12 periods in a space of 1 unit on the time axis. For this to agree with what we know about the sun, I would expect there to be 12 periods in a space of 2 units on the time axis. From Figure 4.6 it can be seen that this is the case and my results agree with the observed data.

Figure 4.7 shows the torsional oscillations for $D = -1000$ and $\tau = 0.025$. Clearly this does not look as expected. When considering the torsional oscillations, we expect a steady mode along with the excited parts. It is difficult to remove the long time-scale modulation from the values to see the underlying structure. For this example, the graph could be improved only looking at a very short time-scale but this problem is one of the limitations of time-averaging.

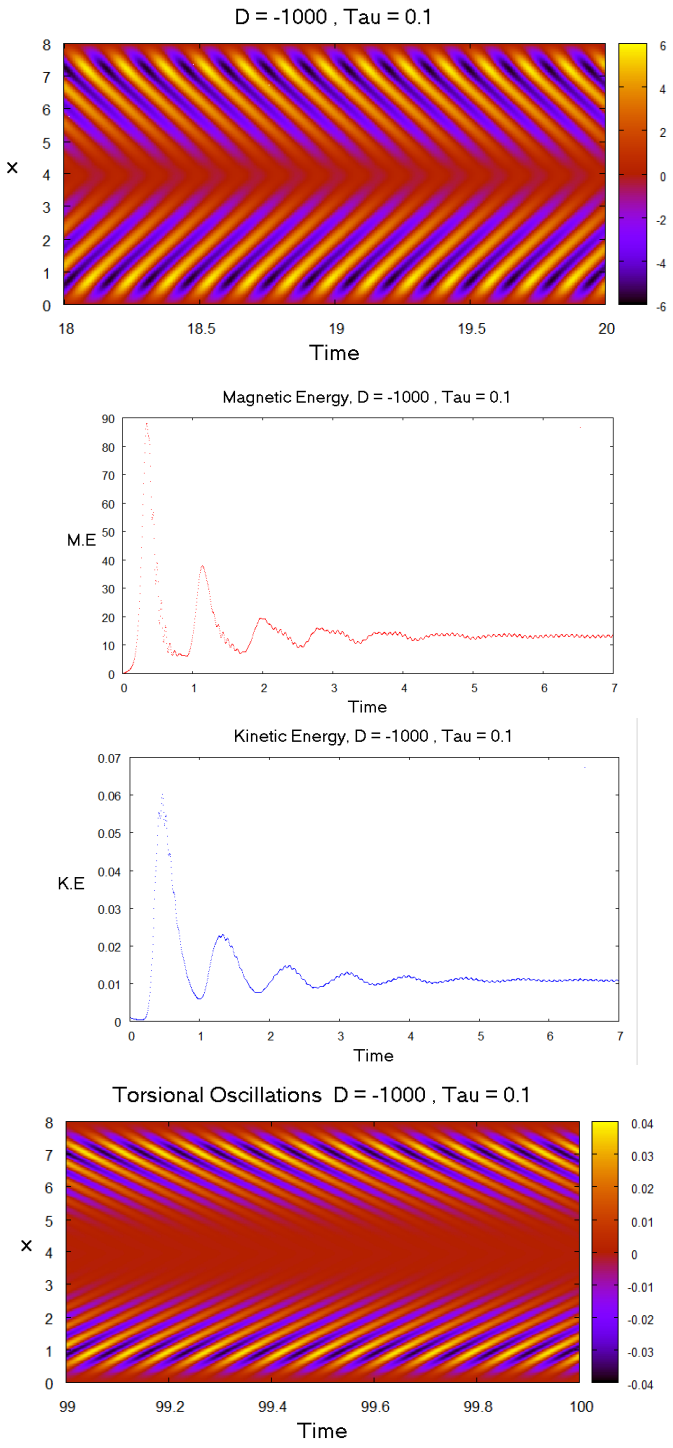

Figure 4.6: Top: Contours of B_1 and x over time when $D = -1000$ and $\tau = 0.1$. Middle: Magnetic energy (red), Kinetic energy (blue). Bottom: Torsional oscillations.

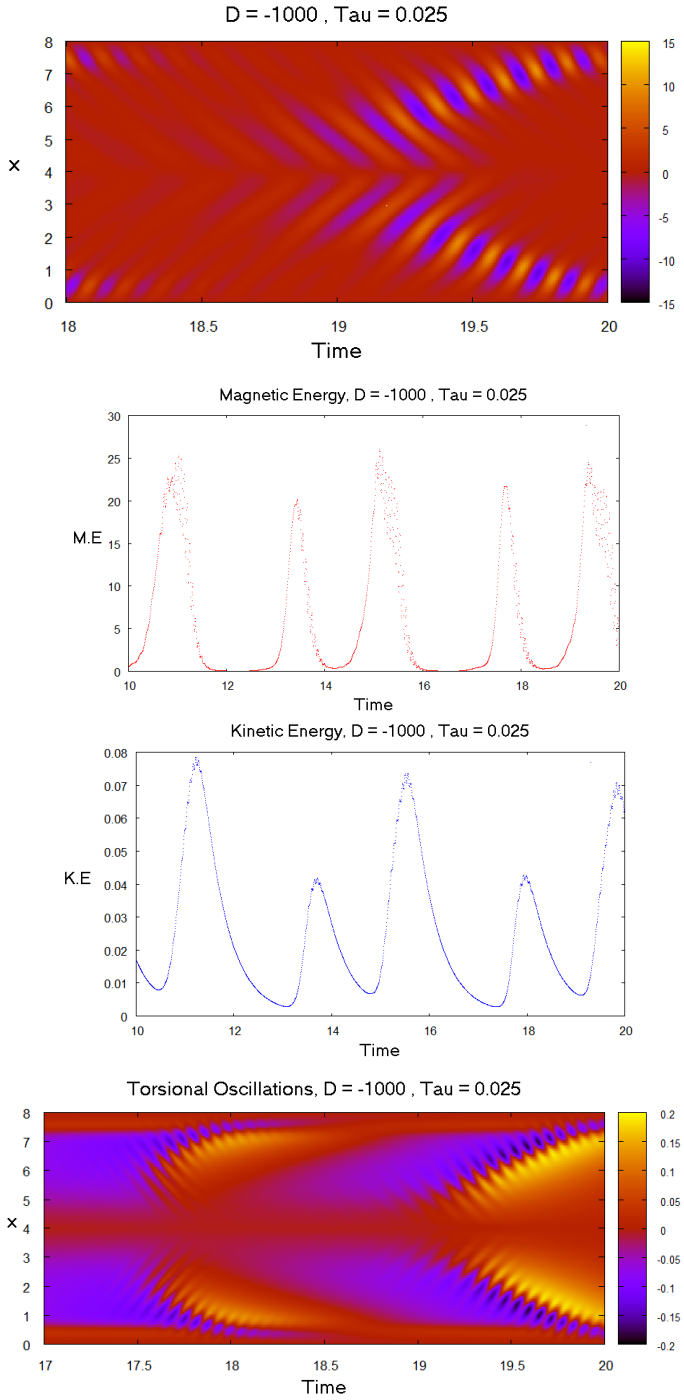

Figure 4.7: Contours of B_1 and x over time when $D = -1000$ and $\tau = 0.025$. Middle: Magnetic energy(red), Kinetic energy (blue). Bottom: Torsional oscillations

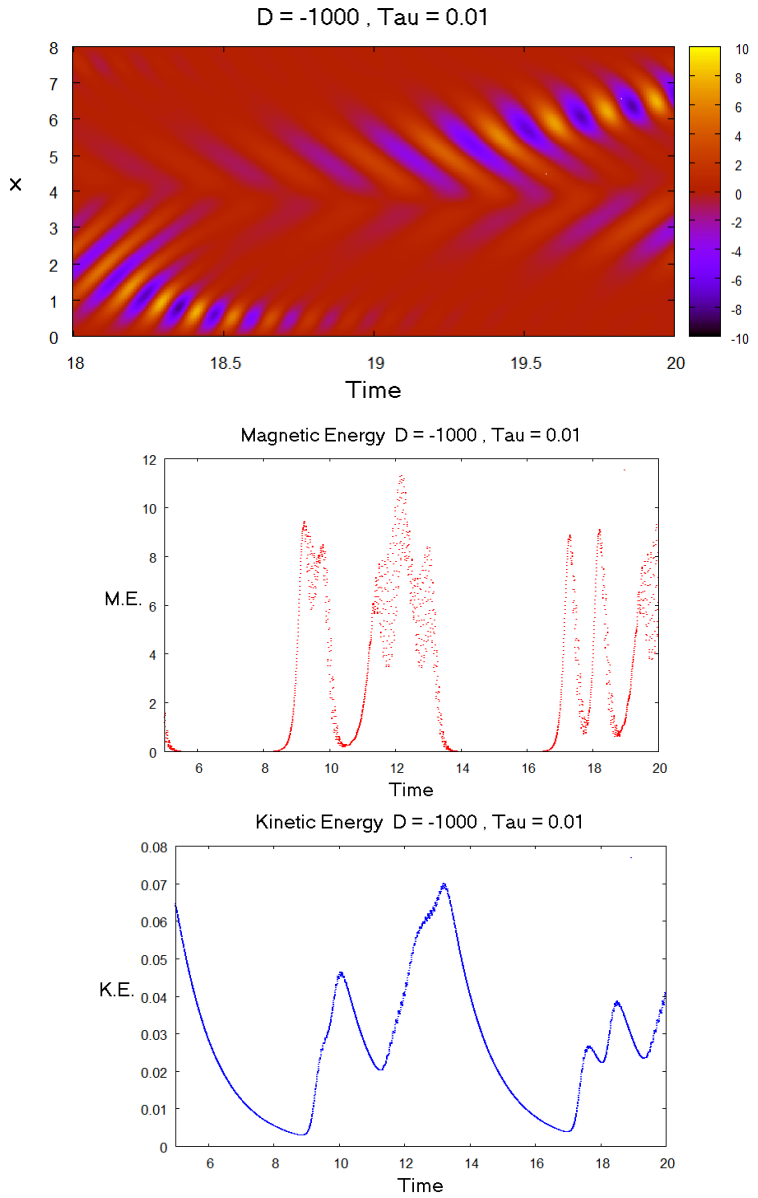

Figure 4.8: Contours of B_1 and x over time when $D = -1000$ and $\tau = 0.01$. Middle: Magnetic energy. Bottom: Kinetic energy

Chapter 5

Sixth Order System

5.1 Model Equations

To create a more realistic model, I changed $f(x, z)$ to allow for increasing and α with z, representing increasing turbulence:

$$f(x,z) = \frac{F(x)}{2}\left[1 - \cos(\pi z)\right]. \tag{5.1}$$

This requires a new Ansatz:

$$A(x,z,t) = A_1(x,t)\sin(\pi z) + A_2(x,t)\sin(2\pi z), \tag{5.2}$$

$$B(x,z,t) = B_1(x,t)\sin(\pi z) + B_2(x,t)\sin(2\pi z), \tag{5.3}$$

$$V(x,z,t) = V_1(x,t)\sin(\pi z) + V_2(x,t)\sin(2\pi z), \tag{5.4}$$

which results in six equations:

$$\frac{\partial A_1}{\partial t} = \frac{F(x)}{2}B_1 - \frac{F(x)}{4}B_2 + \frac{\partial^2 A_1}{\partial x^2} - \pi^2 A_1, \tag{5.5}$$

$$\frac{\partial A_2}{\partial t} = \frac{F(x)}{2}B_2 - \frac{F(x)}{4}B_1 + \frac{\partial^2 A_2}{\partial x^2} - \pi^2 A_2, \tag{5.6}$$

$$\frac{\partial B_1}{\partial t} = D\frac{\partial A_1}{\partial x} + \pi D\left[-V_2\frac{\partial A_1}{\partial x} + \frac{V_1}{2}\frac{\partial A_2}{\partial x} - \frac{A_1}{2}\frac{\partial V_2}{\partial x} + A_2\frac{\partial V_1}{\partial x}\right] + \frac{\partial^2 B_1}{\partial x^2} - \pi^2 B_1, \tag{5.7}$$

$$\frac{\partial B_2}{\partial t} = D\frac{\partial A_2}{\partial x} + \pi D\left[\frac{V_1}{2}\frac{\partial A_1}{\partial x} - \frac{A_1}{2}\frac{\partial V_1}{\partial x}\right] + \frac{\partial^2 B_2}{\partial x^2} - 4\pi^2 B_2, \tag{5.8}$$

$$\frac{\partial V_1}{\partial t} = \pi sign(D)\left[-B_2\frac{\partial A_1}{\partial x} + \frac{B_1}{2}\frac{\partial A_2}{\partial x} - \frac{A_1}{2}\frac{\partial B_2}{\partial x} + A_2\frac{\partial B_1}{\partial x}\right] + \tau\left[\frac{\partial^2 V_1}{\partial x^2} - \pi^2 V_1\right], \tag{5.9}$$

$$\frac{\partial V_2}{\partial t} = \frac{\pi}{2}sign(D)\left[B_1\frac{\partial A_1}{\partial x} - A_1\frac{\partial B_1}{\partial x}\right] + \tau\left[\frac{\partial^2 V_2}{\partial x^2} - 4\pi^2 V_2\right]. \tag{5.10}$$

As with the 3rd order system, I included commands to calculate the magnetic and kinetic energy. The magnetic energy is found from

$$E_M = \frac{1}{2}\int_0^1\int_0^8 \left[B_1(x,t)\sin(\pi z) + B_2(x,t)\sin(2\pi z)\right]^2 \,\mathrm{d}x\mathrm{d}z, \tag{5.11}$$

which can be simplifed down to

$$E_M = \frac{\Delta x}{4}\sum_{i=1}^{N-1}\left[B_1(i)^2 + B_2(i)^2\right]. \tag{5.12}$$

Similarly,

$$E_K = \frac{1}{2}\int_0^1\int_0^8 \left[V_1(x,t)\sin(\pi z) + V_2(x,t)\sin(2\pi z)\right]^2 \,\mathrm{d}x\mathrm{d}z, \tag{5.13}$$

$$= \frac{\Delta x}{4}\sum_{i=1}^{N-1}\left[V_1(i)^2 + V_2(i)^2\right]. \tag{5.14}$$

5.2 Results

Beginning with trying to find the critical value for D, I let $\tau = 1$ as with the third order system and varied D. From Figure5.1 it can be seen that the critical value for D is approximately -1100. Here the contours are clearly symmetric and periodic with an amplitude of around 15. The factor of $[1-\cos(\pi z)]$ in $f(x,z)$ means that it will always be less than the alpha for the 3rd order system and so this system will have to work harder to drive a dynamo. This explains why the critical D value is greater in modulus than that for the 3rd order system.

Keeping τ constant and decreasing D to -2000, as in Figure 5.2, the contours of B1 are still symmetric but are no longer completely periodic, there is some modulation. Some of the cycles appear weaker than others. Again the amplitude is approximately 15.The values of magnetic energy reflect that the cycles are no longer periodic. Now decreasing D to -3000, Figure 5.3 shows clear modulation. Again, the contours seem to be roughly symmetric about

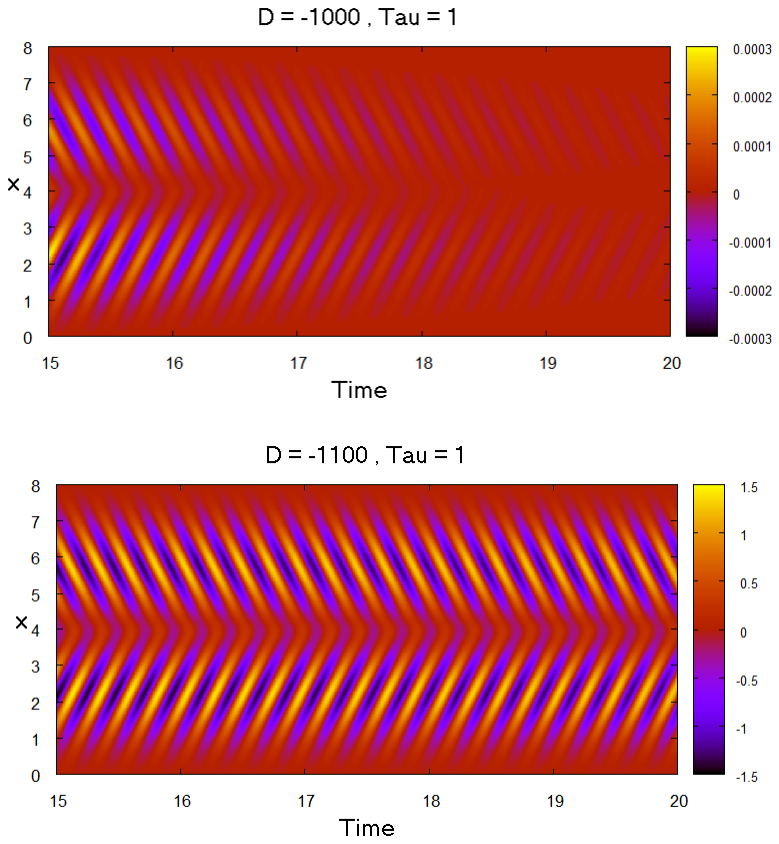

Figure 5.1: Contours of B_1 and x over time. Top: $D = -1000$, $\tau = 1$. Bottom: $D = -1100$, $\tau = 1$

the equator but now have an amplitude of 25. The magnetic energy values range from 140 to 220 which a massive increase from the previous plot. One point of interest when comparing this plot to Figure 5.2 is that the the plot showing a smaller D value is actually more complicated. I would expect that as the modulus of D increases the complexity of the contours will increase. There is obviously some form of non-trivial D dependence for the 6th order system, this may simply be a quirk of my model.

As with the 3rd order system, the effects of decreasing tau can be shown. Starting with $D = -1500$ and $\tau = 0.5$ in Figure 5.4 the contours of B1 are periodic and symmetric about the equator with an amplitude of 8. Decreasing τ to 0.1, Figure 5.5 shows that the contours are no longer symmetric and the amplitude has decreased to 3. Figure 5.6 shows the case when $\tau = 0.01$. The contours are now completely aperiodic and the amplitude has decreased once again to 1. This decrease in amplitude is expected as a smaller τ inhibits the dynamo. I would also have expected to see some modulation at such a low τ but it may be that D also needs to decrease to see such results.

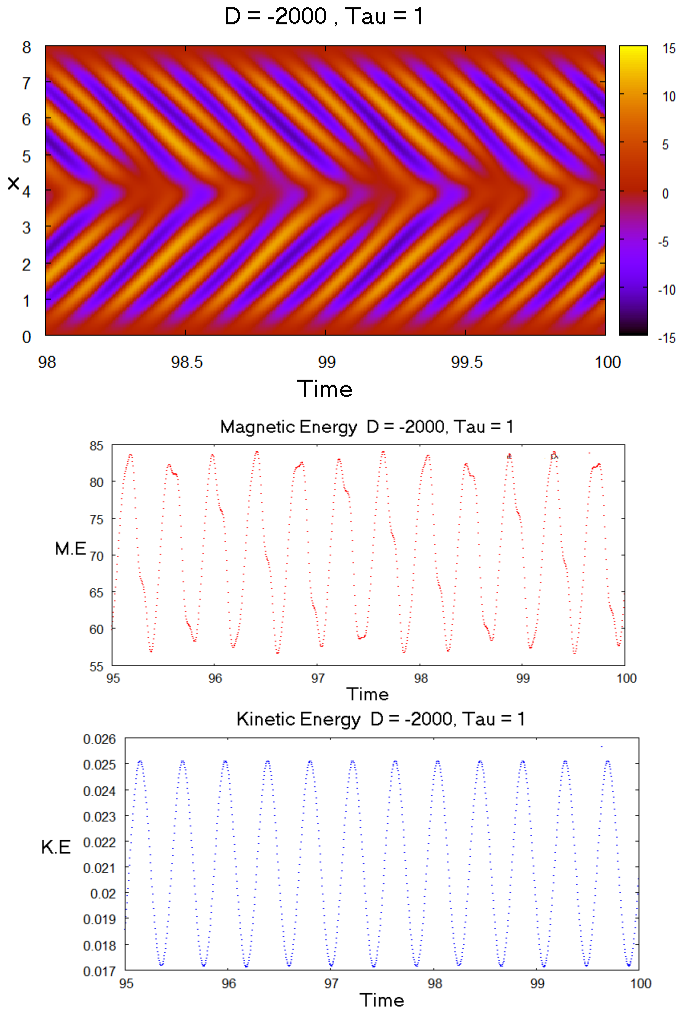

Figure 5.2: Contours of B_1 and x over time when $D = -2000$ and $\tau = 1$. Middle: Magnetic energy. Bottom: Kinetic energy

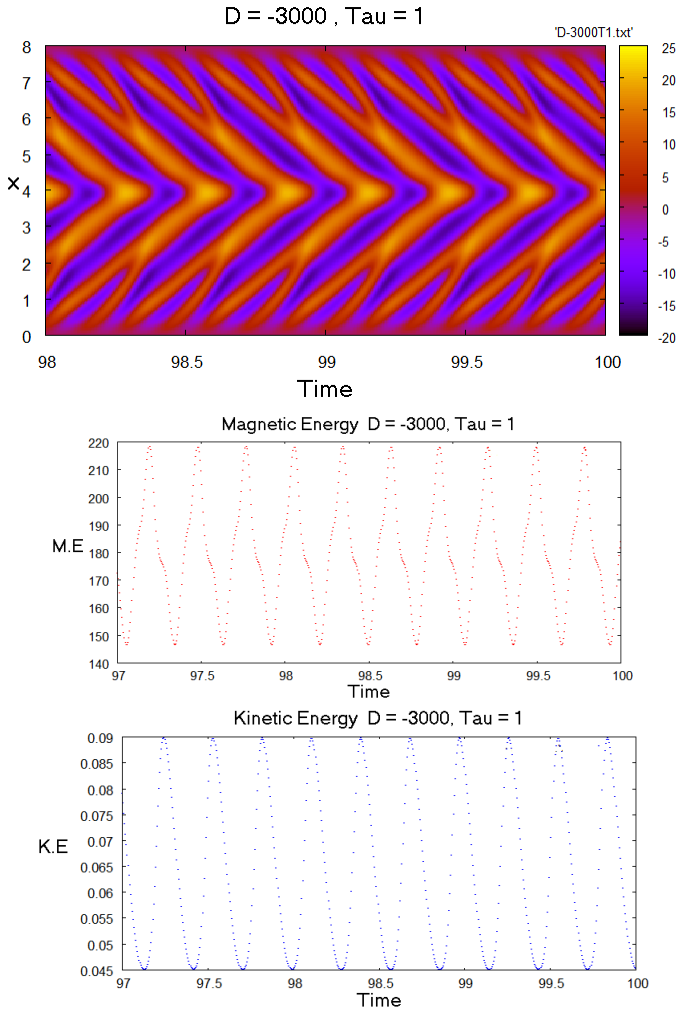

Figure 5.3: Contours of B_1 and x over time when $D = -3000$ and $\tau = 1$. Middle: Magnetic energy. Bottom: Kinetic energy

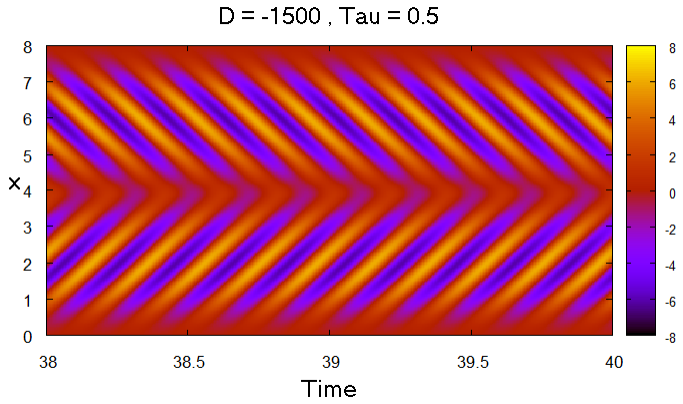

Figure 5.4: Contours of B_1 and x when $D = -1500$ and $\tau = 0.5$

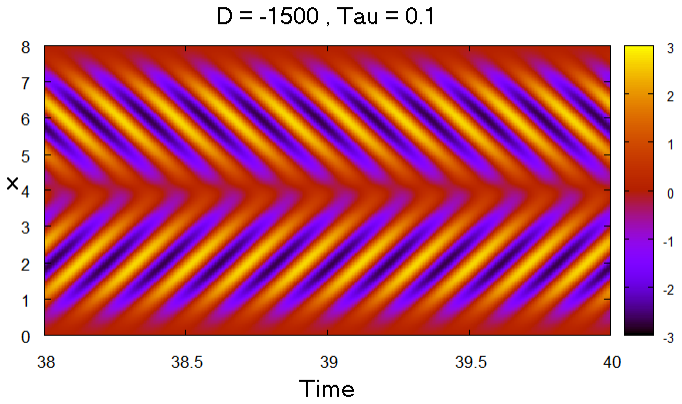

Figure 5.5: Contours of B_1 and x when $D = -1500$ and $\tau = 0.1$

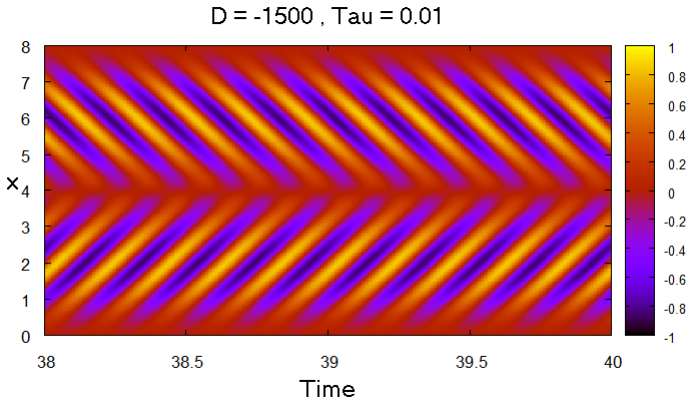

Figure 5.6: Contours of B_1 and x when $D = -1500$ and $\tau = 0.01$

Chapter 6

Conclusions

I have found the method of using an interface dynamo to be quite successful in recreating the Sun's magnetic field. Obviously my simplified 2 dimensional model will not produce as accurate result as a full spherical model but I am happy that my model has produced results that are concurrent with the Sun. My own butterfly diagrams are clearly very similar to butterfly diagram of sunspots observed on the Sun.

Starting with the simpler third order system I first found that for positive D the direction of propagation for the contours of B_1 is opposite to that observed on the Sun and so not of real interest to me. Next, I found that for negative D the direction of propagation now agrees with the observations from the Sun and the critical value of D for the onset of dynamo action is approximately -450. When $\tau = 1$ decreasing D causes the contours to become less symmetric and periodic. The values of magnetic energy and kinetic energy also vary more, over a larger scale, as D decreases. Next, keeping $D = -1000$ and decreasing τ from 0.1 to 0.01 causes the contours to become increasingly aperiodic and showing modulation.

Increasing the complexity with the sixth order system the critical D value is now approximately -1100. Again keeping $\tau = 1$ and decreasing D leads to quite complex contours of B_1 and energy plots. Then keeping D constant at -1500 clearly shows that as τ decreases, the contours remain periodic but become completely asymmetric.

In the future I would like to continue on with my work the torsional oscillations. Further I would continue work on the linear theory using Matlab to find a value for critical D. I would then consider the 4-mode case and even the 6-mode case. This should increase the accuracy of the critical D value. Finally, I would also like to consider more complicated models, perhaps using a Fourier expansion in the horizontal plane.

Bibliography

Charbonneau, P. 2010 Dynamo Models of the Solar Cycle. *Living Reviews in Solar Physics* **7**, 3.

Dawes, J. H. P. 2007 Localized convection cells in the presence of a vertical magnetic field. *Journal of Fluid Mechanics* **570**, 385–406.

Dikpati, M., de Toma, G. & Gilman, P. A. 2006 Predicting the strength of solar cycle 24 using a flux-transport dynamo-based tool. *Geophysical Research Letters* **33**, 5102.

Press, W. H. *et al.* 1986 Numerical recipes : the art of scientific computing .

Schou, J. *et al.* 1998 Helioseismic Studies of Differential Rotation in the Solar Envelope by the Solar Oscillations Investigation Using the Michelson Doppler Imager. *ApJ* **505**, 390–417.

Sokoloff, D. & Nesme-Ribes, E. 1994 The Maunder minimum: A mixed-parity dynamo mode? *A&A* **288**, 293–298.

Stix, M. 2002 *The sun: an introduction*.

Tobias, S. M. 1996 Grand minimia in nonlinear dynamos. *A&A* **307**, L21.

Tobias, S. M. 2002 The solar dynamo. *Royal Society of London Philosophical Transactions Series A* **360**, 2741–2756.

Vorontsov, S. V., Christensen-Dalsgaard, J., Schou, J., Strakhov, V. N. & Thompson, M. J. 2002 Helioseismic Measurement of Solar Torsional Oscillations. *Science* **296**, 101–103.